

# Flood extent delineation in Mozambique after Cyclone Idai using Sentinel-1 data

Julia Janicki

## Introduction

Floods are among the most frequent and devastating natural disasters in the world, greatly impacting human lives and causing great economic damage (**Sanyal & Lu 2004**). About 1.4 billion people were affected by floods and 100,000 have lost their lives over the decade of 1990s (**Jonkman & Kelman 2005**).

The situation will only get worse both regionally and globally; projected increases in the frequency and intensity of rainfall based on climate models indicate increases in precipitation-generated local flooding (**Kundzewicz et al. 2014**). Cyclone Idai is a really good demonstration of this phenomenon. It made landfall in Mozambique on March 14, 2019 and is the second-deadliest tropical cyclone recorded in the South-West Indian Ocean basin, only behind the 1892 Mauritius cyclone. The United Nations estimated that Cyclone Idai and subsequent flooding destroyed more than 1 billion USD worth of infrastructure. Over 100,000 homes were damaged or destroyed, at least 1 million acres of crops were destroyed, and over 1000 people were killed across Mozambique, Zimbabwe and Malawi (**Bearak 2019**).

Flood mapping has played an important role in flood prevention and mitigation, as well as in devising emergency responses. Satellite remote sensing has become a common tool used for flood mapping and it has progressed from using optical images to delineate floods to predicting flood extent as well as using radar images to obtain data during a flood. Now real-time or near real-time flood mapping has become feasible, and it has also become more crucial with the ever increasing number of tropical storms and hurricanes.

One of the most basic but essential applications of remote sensing in flood mapping flood extent delineation, which is often done by using radar data given their cloud penetration capabilities. Flood extent maps derived from SAR data are essential for effective disaster management, as it can provide relief organizations and decision-makers spatial information on flooded areas near real time and in a cost-efficient manner (**Twele et al. 2016**).

In this study I used Sentinel-1 SAR data to delineate flooded areas in the region near Beira, a city in Mozambique that was greatly affected by the flooding from Cyclone Idai. I will also conduct an accuracy assessment by comparing the flood extent from my map to that conducted by UN Operational Satellite Applications Programme (UNOSAP).

## **Background**

Traditionally, common methods of flood mapping are often based on ground surveys and aerial observations (**Brivio et al. 2000**). However, there are limitations to flood mapping using traditional methods, since such methods are time-consuming and expensive when the flood is widespread, and in general more remote places tend to be difficult to access. Moreover, obtaining information during extreme flooding could be challenging due to the unfavorable weather conditions, the possible collapse of communication systems and damage to transportation systems (**Bhatt 2014**).

Satellite remote sensing can solve many of the above problems. Satellites are capable of taking images remotely across a wide range with synoptic views, over multiple and frequent time periods, and of areas that are inaccessible in general or inaccessible during floods. Multi-date imageries can be used to monitor the changes or reconstruct the progress of a past flood (**Sanyal & Lu 2004**).

Remote sensing based flood mapping can be based on either optical data or radar data. Optical remote sensing can only operate effectively during daytime in cloudless conditions. Radar sensors are active sensors that pulse a radar beam to the earth's surface then register the backscattered signal at a receiving unit. Thus radar data be used for flood monitoring even when cloud cover is present and in bad weather conditions, making radar systems the preferred tools for flood mapping (**Schumann et al. 2010**).

## **Study Area**

The study area takes place in the Sofala province in Mozambique and includes regions that were the most affected by Cyclone Idai. These regions include the port cities Beira and Nova Sofala, the city Dondo, as well as areas along the Buzi river (**Figure 1**).

## **Methods**

### SAR preprocessing

Two Sentinel-1 Level-1 Detected High-Res Dual-Pol (GRD-HD) products were acquired from the Alaska Satellite Facility's data portal. An image taken by Sentinel-1A was acquired for the date 2019-03-02 at path 6 and frame 659 (**Figure 2**), depicting the study area before the flood. And an image taken by Sentinel-1B was acquired for the date 2019-03-20 at path 6 and frame 657 (**Figure 3**), depicting the study area after the flood. For this study I used the intensity data for the VH polarization from the C-band.

First, the SAR intensity data was processed to produce ready-to-use products by using the European Space Agency's SNAP software. To start, radiometric correction was applied to both images by computing the radar backscatter coefficient which characterizes the amount of energy returned to the sensor per unit area. With the backscatter values, the pixel values can be directly related to the radar backscatter of the scene.

Next, since radar images are subject to the speckle effect that degrades the information content and makes image interpretation difficult, speckle reduction techniques are commonly employed, such as using filters. The most commonly used filter is the Lee Sigma Filter (**Lee, 1980**), which first computes the standard deviation for the entire image, then the brightness value within a  $3 \times 3$  moving window is replaced with the average of only those neighboring pixels that have intensity values within two standard deviations of the central pixel.

Finally, SAR images frequently contain spatial distortions as a result of topographical variations across the scene and the tilt of the sensor during acquisition. Accordingly, orthorectification is often necessary for processing SAR images in order to geo-register and geo-rectify the data using a digital elevation model.

### Change Detection

Once the two SAR images were preprocessed, they were brought into ENVI in order to perform a change detection. Image differencing is a technique that can be used for change detection. The image from the earlier date (2019-03-02) was subtracted from the image from the later date (2019-03-20) using Band Math in ENVI in order to obtain a difference image.

Density slicing was then applied to the difference image to create a classified map by using Raster Color Slices. Density slicing is done by dividing the range of brightnesses in a single band into intervals, then assigning each interval to a color. Various colors slices were created based on histogram values: -781 to -1, -1 to -0.5, -0.5 to -0.05, -0.05

to 0, 0 to 0.5, 0.5 to 1, 1 to 1341. The classes were then combined to produce two final classes that are relevant for the purpose of this project: flooded areas (-1 to -0.05) and non-flooded areas (the rest of the values).

### Accuracy Assessment

The first step is to select a sample design for creating testing sites. In general, random points are better than non-random points since it would be governed by chance and each point has an equal likelihood of being represented. It is also better to choose a sample of certain number of points instead of comparing all the points, otherwise it will take too long. A random sample design was chosen given that the study area does not have a lot of variability in specific areas.

Ninety-nine testing pixels were generated randomly from a noise image for the two images to create the testing data. The testing data was then labeled by using the flood extent map generated by UNOSAP as a reference. The test data was labeled into two classes: flooded areas and non-flooded areas.

An error matrix was produced by comparing the randomly generated “ground truth” test pixels to the land cover type classes produced in the final images by using the “Confusion Matrix Using Ground Truth ROIs” function in ENVI, including total accuracy, user’s accuracy and producer’s accuracy.

### **Results**

The differences between two images visualized using RGB composites can be seen in **Figure 4** and the final flood extent map can be seen in **Figure 5**. At the end there were two land cover type classes: flooded areas and non-flooded areas. The error matrix for the map resulting from the density slicing method can be seen in **Table 1**. The overall accuracy for the image is 90.9091% (90/99) and the kappa coefficient is 0.7266.

The non-flood class has very highest user’s accuracy at 100%, which means that users would find that 100% of the time when they visit this area that what the classified map calls “non-flooded” will actually be areas that are not flooded. It also has pretty high producer’s accuracy at 89%, which means that most of the flooded areas have been correctly identified as “flooded”, some areas that should have been classified as flooded areas were misclassified as non-flooded areas.

### **Discussion**

The overall accuracy of the flood delineation using the density slicing method is generally very satisfactory, but further improvements could be made to better classify the image. Different polarizations, bands, or data from different satellites or different indices can be used to attempt to improve accuracy.

For Sentinel-1 data, slightly higher thematic accuracies can be achieved by using VV instead of VH polarizations (**Twele et al. 2016**). Other satellites such as TerraSAR-X permits the acquisition of HH-polarized data, which are generally considered as superior to other polarizations in the context of flood mapping.

Moreover, X-band data can be used instead of C-band data for higher accuracy. In comparison to X-band SAR data from satellites such as TerraSAR-X or Cosmo-SkyMed, the system parameters of Sentinel-1 tend to be more challenging for mapping water surfaces. As the contrast between non-water and water areas decreases with increasing wavelength of the SAR system (**Drake and Shuchman 1974**), lower classification accuracies are expected for C-band Sentinel-1 data.

Different indices could also be used to potentially improve the results. The Normalized Difference Water Index (NDWI) is derived from the Near-Infrared (NIR) and green channels (**McFeeters 1996**) and is efficient for detecting water surfaces since these surfaces have very low reflectance in the NIR region of the spectra. In order to achieve higher over accuracy, NDWI can first be calculated for both the before and after images, then the density slicing method can applied to the difference image of the NDWI images.

Finally, there are many algorithms that have been developed for the purpose of change detection and could produce better results than using density slicing. Some algorithms developed for mapping flooded areas for change detection purposes for SAR images include the KIGG algorithm (**Bazi et al. 2005**) and HSBA-Flood algorithm (**Chini et al. 2017**).

## **Conclusion**

The study demonstrates that flood extent delineation can be successfully done by using time series Sentinel-1 data, and that density slicing is a good option when it comes to methods for conducting change detection.

The final flood map successfully identifies most of the inundated areas, with an overall accuracy of 90.9091%. The results could potentially be improved by using VV or HH polarizations instead of VH, using different types of imagery or bands such as the X-band from a different satellite, using indices such as NDWI, or using different algorithms to detect flooded areas.

## Figures and Tables

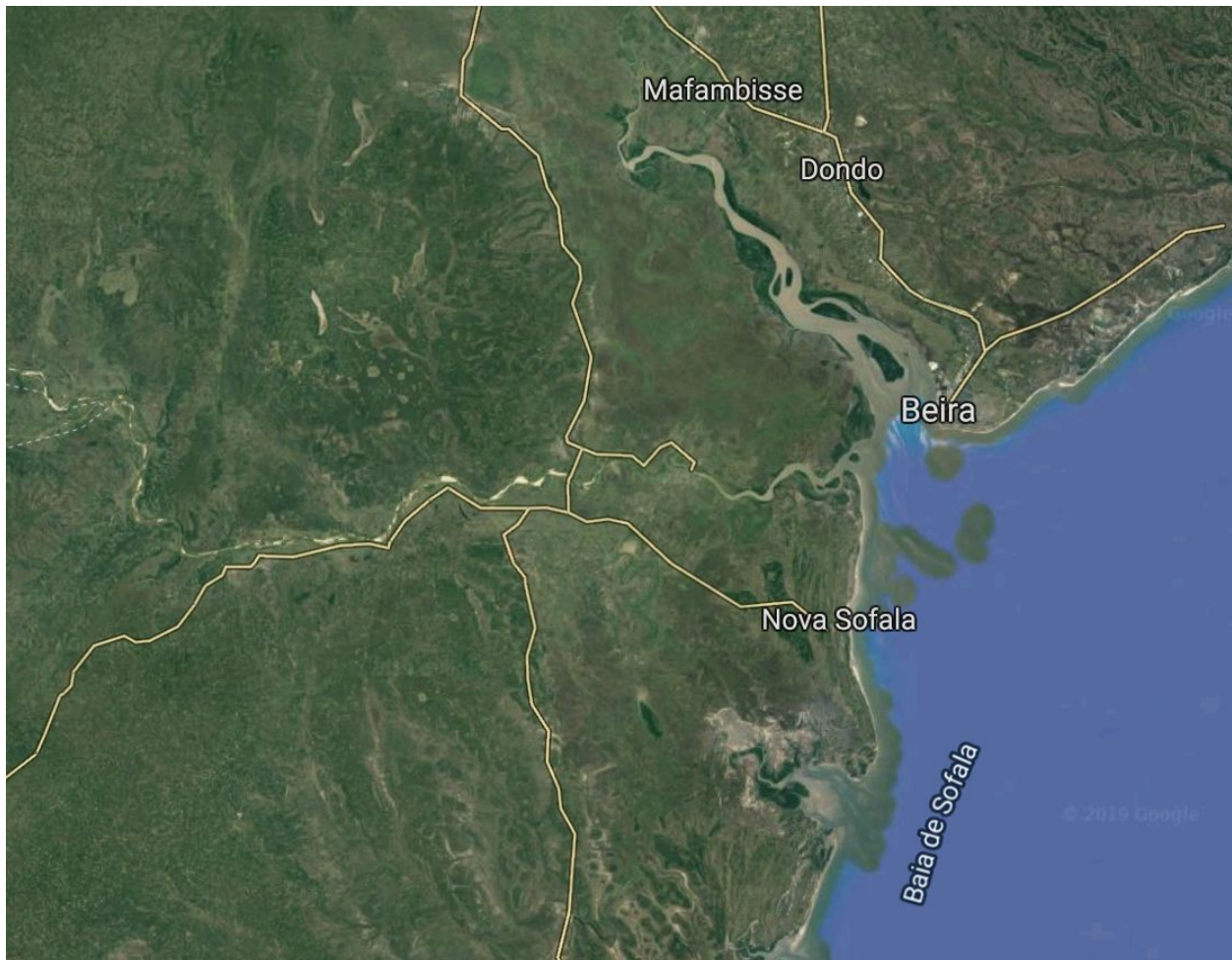


**Figure 1.** Optical image of study area, taken from the satellite view of Google Maps, based on Landsat 8 data.

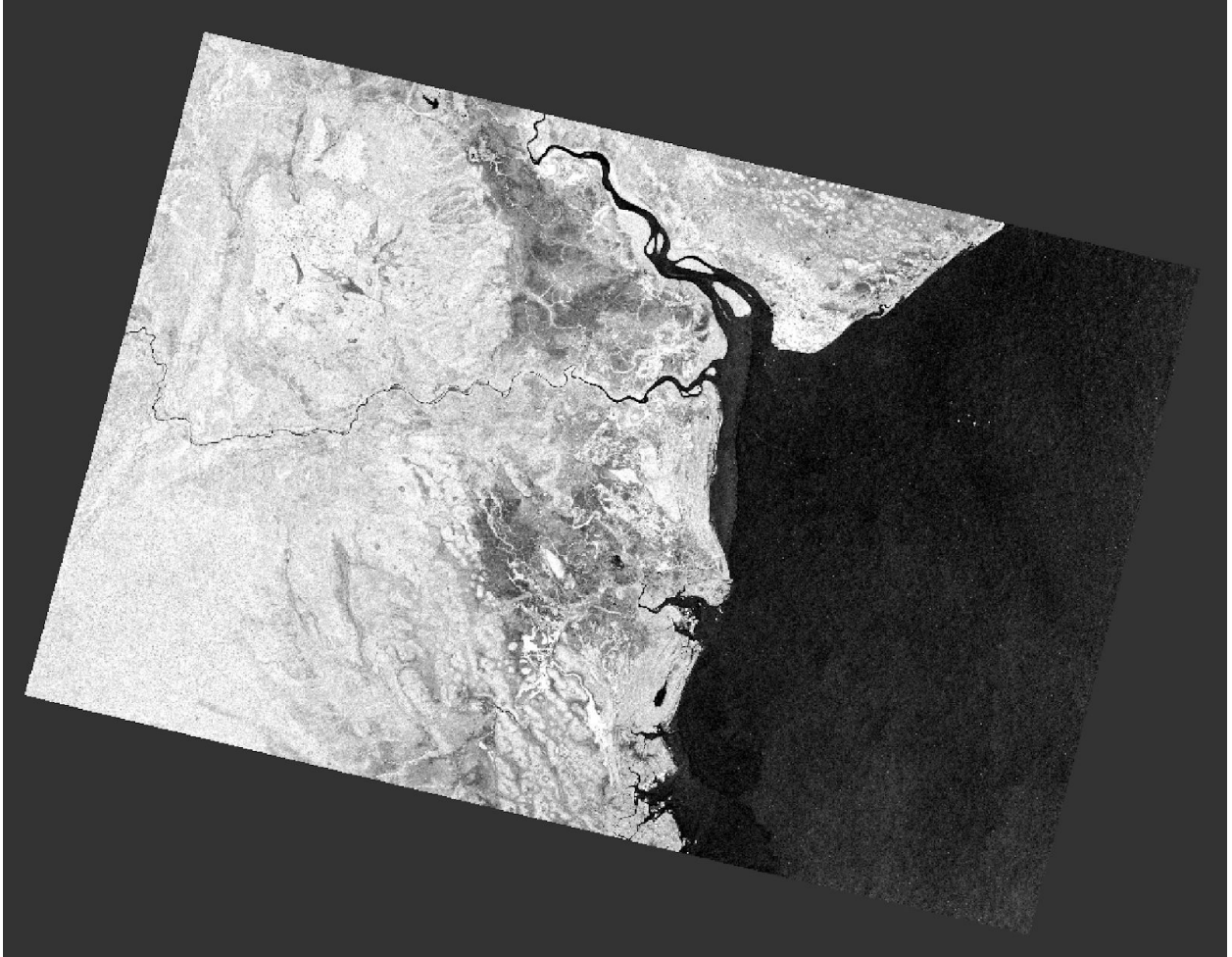


**Figure 2.** The study area before the flood. Image taken by Sentinel-1A's C-band on the date 2019-03-02 at path 6 and frame 659. The intensity values of the VH polarization was radiometrically corrected, speckled filtered and terrain corrected.

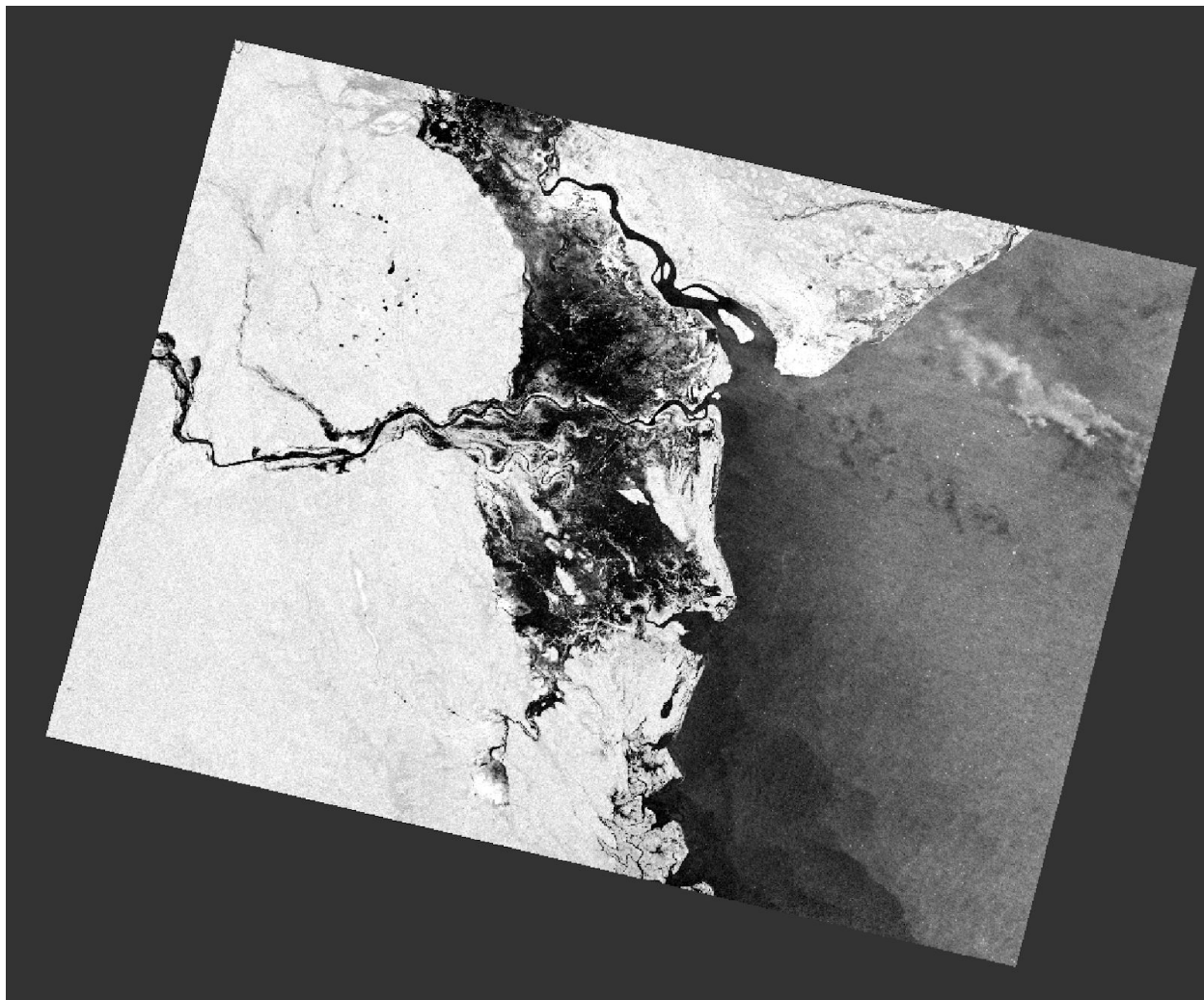


**Figure 3.** The study area after the flood. Image taken by Sentinel-1B's C-band on the date 2019-03-20 at path 6 and frame 657. The intensity values of the VH polarization was radiometrically corrected, speckled filtered and terrain corrected.

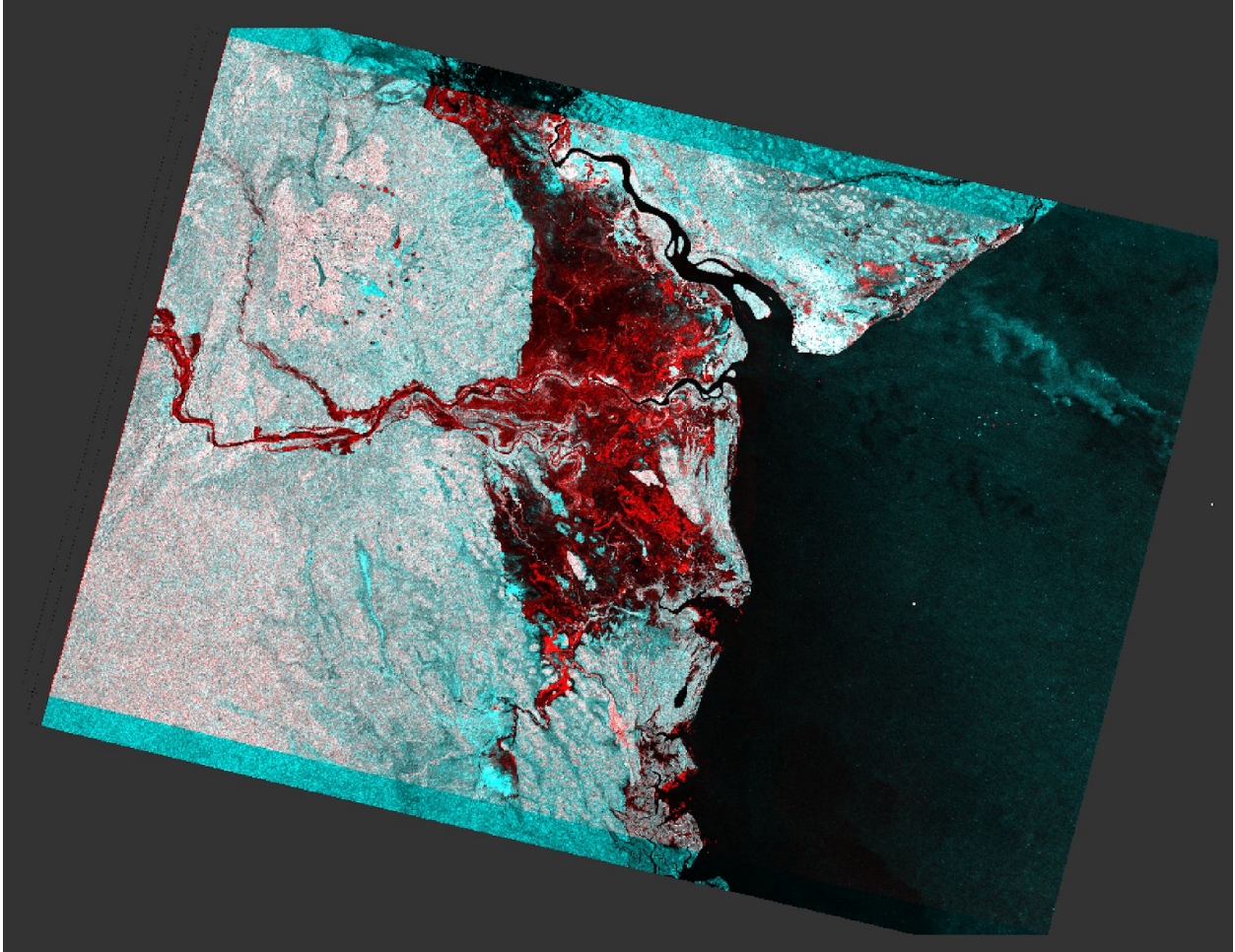


**Figure 4.** The RGB composites of the before flood and after flood images. The green and blue channels display the before image while the red channel displays the after image, which is why the flooded areas are displayed in red.

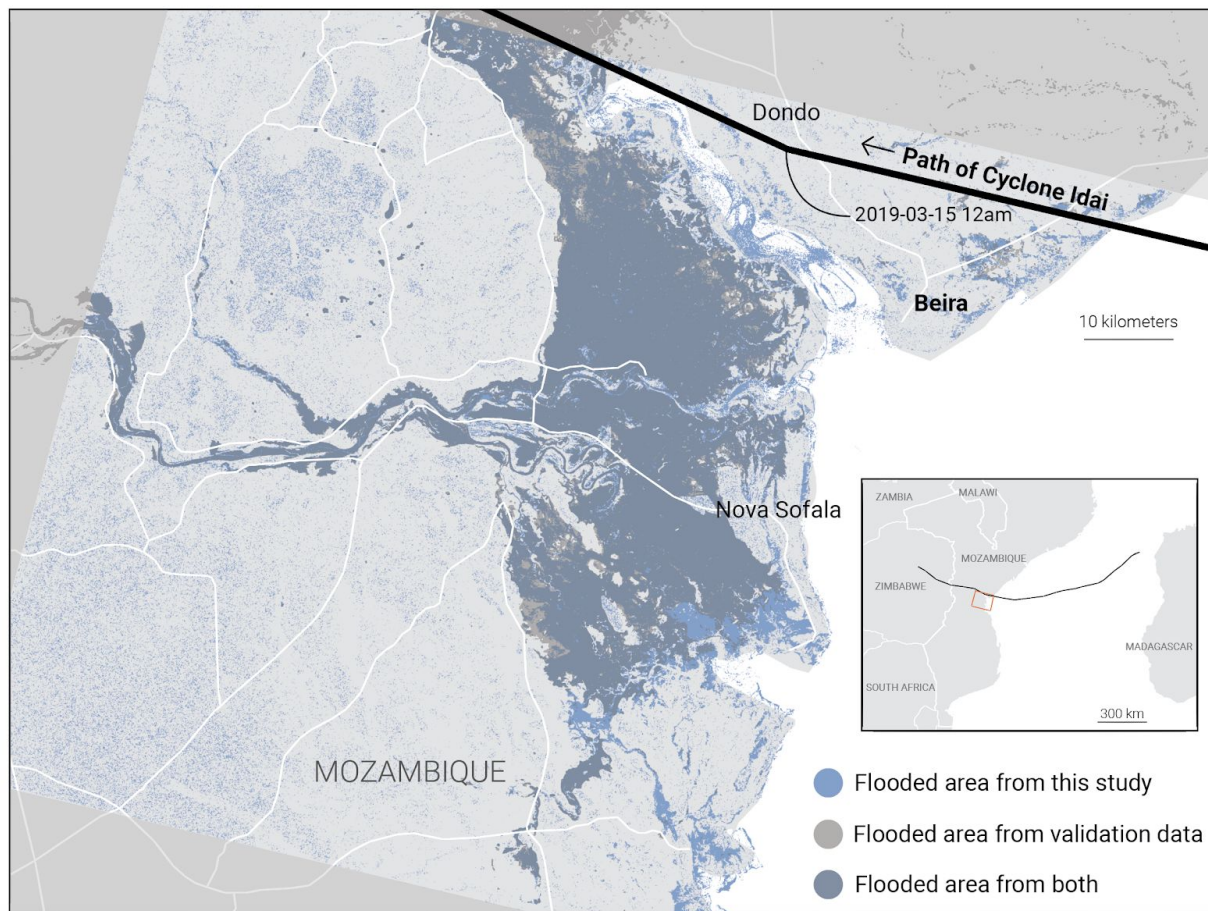


**Figure 5.** The final classified map that displays flooded areas by using density slicing for mapping change detection in an area in Mozambique that was most affected by Cyclone Idai. The flood extent mapped by UNOSAP (validation data) is also displayed for comparison.

<b>Class</b>	<b>non-flood</b>	<b>flood</b>	<b>Total</b>	<b>User's accuracy</b>
<b>non-flood</b>	74	0	74	100%
<b>flood</b>	9	16	25	64%
<b>Total</b>	83	16	99	
<b>Producer's Accuracy</b>	89%	100%		

**Table 1.** Error matrix for the final classified map based on density slicing of the difference image, displaying the flooded areas and non-flooded areas.

## Reference

- Bazi, Y., Bruzzone, L. & Melgani, F. 2005. An unsupervised approach based on the generalized Gaussian model to automatic change detection in multitemporal SAR images. *IEEE Transactions on Geoscience and Remote Sensing* 43 (4): 874–887, Apr. 2005.
- Bearak, M. 2019. ‘Everything is destroyed’: Mozambique fears massive human toll from Cyclone Idai. *The Washington Post*. Retrieved 19 March 2019.
- Bhatt, C. M. & Rao, G. S. 2014. Ganga floods of 2010 in Uttar Pradesh, north India: a perspective analysis using satellite remote sensing data. *Geomatics, Natural Hazards and Risk* 7 (2): 747-763, 2016, <http://dx.doi.org/10.1080/19475705.2014.949877>
- Brivio, P. A., Colombo, R., Maggi, M. & Tomasoni, R. 2002. Integration of remote sensing data and GIS for accurate mapping of flooded areas. *International Journal of Remote Sensing* 23 (3): 429-441, 2002
- Chini, M., Hostache, R., Giustarini, L. & Matgen, P. 2017. A hierarchical split-based approach for parametric thresholding of SAR images: Flood inundation as a test case. *IEEE Transactions on Geoscience and Remote Sensing* 55 (12): 6975–6988, Dec. 2017.
- Drake, B. & Shuchman, R. A. 1974. Feasibility of Using Multiplexed SLAR Imagery for Water Resources Management and Mapping Vegetation Communities. *Proceedings of the 9th International Symposium on Remote Sensing of Environment*, Environmental Research Institute of Michigan, Ann Arbor, MI, April 15–19, 219–249. doi:10.1080/01431161.2015.1060647.
- Jonkman, S. N. & Kelman, I., 2005. An analysis of the causes and circumstances of flood disaster deaths. *Disasters*, 29 (1): 75–97, 2005
- Kundzewicz, Z. W., Kanae, S., Seneviratne, S. I, Handmer, J., Nicholls, N., Peduzzi, P., Mechler, R., Bouwer, L. M., Arnell, N., Mach, K., Muir-Wood, R., Brakenridge, G. R., Kron, W., Benito, G., Honda, Y., Takahashi, K. & Sherstyukov, B., 2013. Flood risk and climate change: global and regional perspectives. *Hydrological Sciences Journal*, 59 (1) 2014
- Lee, J. 1980. Digital Image Enhancement and Noise Filtering by Use of Local Statistics. *IEEE Transactions on Pattern Analysis and Machine Intelligence* PAMI-2(2):165 -168

DOI: 10.1109/TPAMI.1980.4766994

McFeeters, S. K. 1996. The use of the Normalized Difference Water Index (NDWI) in the delineation of open water features. *International Journal of Remote Sensing* 17 (7): 1425-1432.

Sanyal, J., & Lu, X. X., 2004. Application of Remote Sensing in Flood Management with Special Reference to Monsoon Asia: A Review. *Natural Hazards* 33: 283–301, 2004

Schumann, G., Di Baldassarre, G., Alsdorf, D. & Bates, P. D. 2010. Near Real-Time Flood Detection in Urban and Rural Areas Using High Resolution Synthetic Aperture Radar Images. *Water Resources Research*, 46: W05601, doi:10.1029/2008WR007672, 2010

Twele, A., Cao, W., Plank, S. & Martinis, S. 2016. Sentinel-1-based flood mapping: a fully automated processing chain, *International Journal of Remote Sensing* 37 (13): 2990-3004, DOI: 10.1080/01431161.2016.1192304